JOURNAL OF MAGNETIC RESONANCE **132,** 167–171 (1998)
ARTICLE NO. MN981386

Double and Triple Resonance Circuits for High-Frequency Probes

Q. W. Zhang,* Huiming Zhang,*,† K. V. Lakshmi,*,[1] D. K. Lee,*,[2] C. H. Bradley,‡ and R. J. Wittebort*

*Department of Chemistry, University of Louisville, Louisville, Kentucky 40292; †Center for MR Research, Northwestern University, 1033 University Place, Suite 150, Evanston, Illinois 60201; and ‡Anasazi Instruments, 4101 Cashard Lane, Suite 103, Indianapolis, Indiana 46203

Received January 14, 1997; revised December 31, 1997

Heteronuclear solid-state NMR experiments applied to biological macromolecules require an efficient probe which is double or triple tuned for irradiation of two or three nuclei. It should generate intense RF fields without sacrificing sensitivity for the observed nucleus, typically not protons. The purpose of this paper is to describe our approach to building efficient, single-coil double- and triple-tuned probes that are well adapted to the higher frequencies (^{1}H frequency $>$ 400 MHz) currently in use. The number of components and physical dimensions are reduced, thereby decreasing distributed inductance and capacitance, which improves efficiency. Also, transmission lines and their attendant capacitance are removed, which substantially increases the upper frequency limit of the ^{1}H channel to 950 MHz.

Summarized in Fig. 1 is the evolution of the circuit from the double resonance probe introduced by Cross *et al.* (*1*), Fig. 1a, to essentially the one used here, Fig. 1d. The circuit in Fig. 1a uses ^{1}H quarter-wavelength ($\lambda/4$) transmission lines to isolate the high- and low-frequency circuits. It has been simplified by eliminating the open $\lambda/4$ cable (*2*), which is unnecessary since the large tuning capacitance in the low-frequency circuit, C_2, effectively grounds the sample inductor at the ^{1}H frequency.

In a further modification, the $\lambda/4$ transmission lines are replaced with lumped elements (*3, 4*). With the open $\lambda/4$ line eliminated and the shorted $\lambda/4$ line replaced by a lumped-element analog, the circuit is shown in Fig. 1b. By analogy with the shorted $\lambda/4$ line, the inductance, L_G, and capacitance, C_G, are chosen to resonate at the ^{1}H frequency ($L_G\, C_G = 1/\omega^2_H$), thereby providing high- and low-impedance paths to ground at the high and low frequencies, respectively.

To directly compare the circuit of Fig. 1a with one in which the transmission line is replaced by a parallel resonant circuit, Fig. 1b, the inductance and capacitance of the transmission line and the quality factors of both circuits must be known. We do this operationally by comparing the frequency dependence of the impedance of a shorted $\lambda/4$ cable (*5*),

$$Z = Z_0 \tanh\left[\frac{\lambda}{4}\left(\alpha + \frac{i\omega}{\upsilon}\right)\right], \qquad [1]$$

with that for the parallel resonant circuit,

$$Z = \frac{1}{i\omega C + 1/i\omega L + 1/R}. \qquad [2]$$

In Eq. [1], α and υ are the transmission line attenuation factor and propagation velocity (provided by the cable manufacturer and expressed in nepers$\cdot$m^{-1} and m$\cdot$s^{-1}, respectively). In Eq. [2], R is the parallel resistance of the inductor related to the circuit Q by $Q = R/\omega L$. In Fig. 2, the magnitude, $|Z|$, and reactive, Im(Z), parts of the impedance are shown for a 500-MHz shorted $\lambda/4$ cable made from 0.25-inch diameter, Teflon dielectric semirigid coax (UT-250, 4.3 dB attenuation/100 ft and $\upsilon = 2.1 \times 10^8$ m$\cdot$s^{-1}, Uniform Tubing, Collegeville, PA). $Q = 450$ is determined from the resonant frequency divided by the resonant peak width measured at the $0.707|Z|_{peak}$ points. In turn, $L = 20.5$ nH is determined from the resistive resonant impedance, 29.3 kΩ, using $Q = R/\omega L$ and, finally, $C = 4.9$ pF from $\omega = 1/\sqrt{LC}$. With these L, C, and Q values, the impedance for the lumped-element analog, Eq. [2], is superimposed. In the neighborhood of the resonant frequency, the LC circuit and shorted $\lambda/4$ cable are, in practice, equivalent. Well below the resonant frequency, the impedances are somewhat different and the cable inductance, 25 nH, is the value calculated from its length ($\lambda/4$) and inductance per unit length (Z_0/υ) (*6*). The effective inductance of the cable near the resonant frequency is less (by a factor of 0.82), since the dimensions of the device are comparable to the wavelength and the stored energy is somewhat less than at lower frequencies.

To corroborate Eq. [1] and compare quality factors of transmission lines and coils, we have coupled shorted $\lambda/4$ lines and parallel resonant circuits to a 50-Ω bridge via an adjustable capacitor ($Q > 10{,}000$) and measured the width

[1] Present address: Department of Chemistry, Yale University, New Haven, CT.

[2] Present address: Department of Chemistry, University of Michigan, Ann Arbor, MI.

1090-7807/98 $25.00

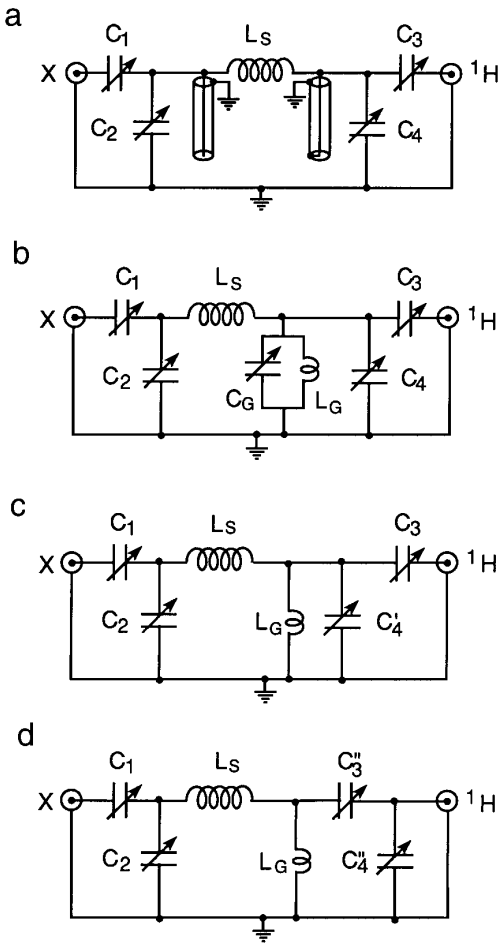

FIG. 1. Double resonance circuits. (a) Circuit due to Cross *et al.* (b) Lumped element version of (a) with the open λ/4 line eliminated. (c) Electrically equivalent to (b) with C_4 and C_G lumped together. (d) Modification of (c) using the same arrangement of inductors.

of the resonance curves. Although this experiment is difficult at 500 MHz since the coupling capacitor is extremely small, we find that at 250 MHz, $Q \sim 220$ for an LC circuit or a 0.141-inch diameter, 250-MHz, shorted λ/4 cable. This is in satisfactory agreement with the value of 240 determined for the transmission line (Eq. [1]). We conclude that the transmission line circuit, Fig. 1a, using component values readily calculated from the known impedance, propagation velocity, and loss of the transmission line, is operationally equivalent to the lumped-element circuit, Fig. 1b.

Independent of the complete probe, the shorted λ/4 line or its lumped-element analog is a resonant circuit at the ^{1}H frequency. When viewed in the complete probe, C_G is in parallel with C_4, i.e., they are a single capacitance (Fig. 1c), and the choice to be made is the inductance L_G, which amounts to a trade-off between the relative efficiencies of the low- and high-frequency channels. With the assumptions that the impedance of C_2 is sufficiently low at the ^{1}H frequency, that of C_3 is sufficiently high at the low frequency, and resistive losses occur primarily in the inductors, the power efficiencies, η_{HF} and η_{LF}, are (*7*)

$$\eta_{HF} = Q_G L_G/(Q_G L_G + Q_S L_S) \text{ and}$$
$$\eta_{LF} = Q_G L_S/(Q_G L_S + Q_S L_G). \quad [3]$$

Whereas increasing L_G improves ^{1}H efficiency, η_{HF}, the opposite increases the low-frequency channel efficiency, η_{LF}, where L_S and L_G are in series. Note that both the low-frequency efficiency and the upper tuning frequency of the ^{1}H channel are increased by decreasing L_G.

Open λ/4 line aside, the circuit in Fig. 1c differs from that in Fig. 1a by replacing the shorted λ/4 transmission line with an inductor. Efficiencies are determined by the inductance and quality factor of the transmission line or the inductor. In practice, *Q*'s for inductors are in the range of 200, whereas *Q*'s in excess of 400 can be obtained with transmission lines. Otherwise, there are two practical advantages to an inductor: It is easily varied so as to control the relative efficiencies of the low- and high-frequency channels, and it adds no capacitance to the ^{1}H resonant circuit. For example, consider a 500-MHz probe with a four-turn, 5-mm sample coil ($L_S \sim 80$ nH). With a shorted λ/4 line, the tuning capacitor has a value near the minimum capacitance

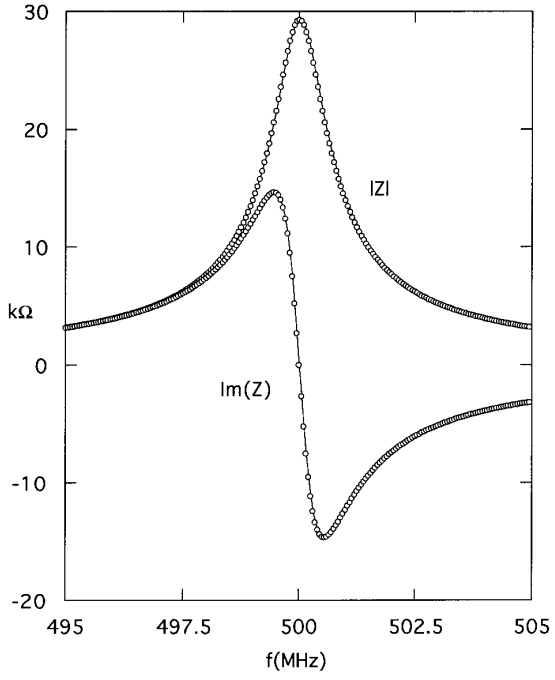

FIG. 2. Frequency dependence of the impedance, *Z*, of a shorted quarter-wave cable (UT-250, Uniform Tubing, Collegeville, PA) and a parallel LC circuit. The magnitude, $|Z|$, and the reactance, Im(Z), of the impedance are traced in open circles for the transmission line and the corresponding values for the LC circuit are superimposed in continuous lines. Component values are given in the text.

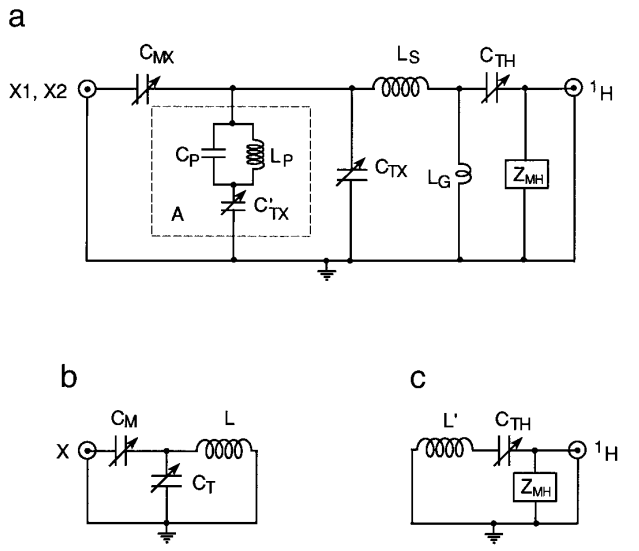

FIG. 3. Double and triple resonance circuit derived from Fig. 1d. The part outlined with dotted lines and labeled A is eliminated in the double-tuned circuit and Z_{MH} is either an inductor or a capacitor.

in available trimmer units, ~1 pF. Upon replacing the transmission line with a 30-nH inductor, the net inductance (L_S and L_G in parallel) is reduced to 22 nH and the tuning capacitance increases to 3.8 pF. Importantly, the circuit can be tuned to substantially higher frequencies.

For purposes of matching the ^1H channel to a 50-Ω load, a further modification is shown in Fig. 1d. A series resonant circuit is used in the ^1H channel. This circuit, implemented as a triple-tuned (^{13}C, ^{15}N, and ^1H) probe used for small powder samples and a broadband double-tuned 500-MHz MAS probe with a 5-mm rotor, is shown in Fig. 3a, and its efficiency is examined experimentally next.

In the MAS probe, gas dielectric (ITT Jennings CHV1, 1.5–45 pF, C_{MX} and C_{TX}) and Teflon dielectric (Voltronics NMNT10-6NL, 1–10 pF, C_{TH}) capacitors were used. The simplicity of the circuit is more fully realized in the triple resonance probe, which uses small capacitors like those found in low power solution NMR probes (variable capacitors: Johanson 52H02, 1–10 pF and chip capacitors ATC 100B). The entire probe circuit is constructed on a single ground plane easily fitting into the 64-mm bore of the 12-tesla magnet. In both probes, potential arcing at the ^1H tuning capacitor was eliminated by placing a 3- to 4-pF chip capacitor in series with C_{TH}. Relative circuit efficiencies were determined by comparing the 90° pulse widths of the double- or triple-tuned probe with those determined when the circuit is reduced to a single-tuned equivalent. Since 90° pulse widths vary linearly with the applied transmitter voltage, efficiencies measured in this way will be the square root of the power efficiencies calculated from Eq. [3].

In Fig. 3a, circuit elements surrounded by dotted lines are eliminated in the double-resonance version, which is described first. As discussed later, the low-frequency, X1, and high-frequency, ^1H, circuits are reasonably approximated by the ''parallel'' or ''series'' resonant circuits shown in Figs. 3b and 3c. Approximate tuning and matching conditions for these circuits are summarized in Table 1.

The probe circuit at the low frequency reduces approximately to a parallel resonant circuit, Fig. 3b. This is tested by replacing L_G with a low-impedance short to ground. With a four-turn solenoidal sample coil (0.2 inch × 0.2 inch and $L_S \sim 80$ nH), the 90° pulse width is 5.5 μs (~125 W at 67 MHz). With the short replaced by a 2.2-turn coil ($L_G \sim 30$ nH), the 90° pulse width increases modestly to 5.7 μs. Thus, double tuning the probe causes a small reduction in the efficiency of the low-frequency channel.

The probe at the ^1H frequency is approximately the ''series'' resonant circuit of Fig. 3c with $L' = L_S L_G/(L_S + L_G)$. At 500 MHz the reactance of the matching component, X_{MH}, is small, making a variable inductor preferable to a large variable capacitor. Using the matching condition for the ^1H channel (Table 1), an inductor with a few nanohenries is needed for typical values of L' and Q'. Compact, low-loss inductors in this range are ''U'' shapes made from 0.004-inch copper foil, Fig. 4 (*8*). The ''U''-shaped coil is soldered onto the PC board and thus physically stable. Figure 4c shows how the inductance is conveniently varied over a range of ~40% by mechanically manipulating the inductor to change the separation between the legs. Note also that L_{MH} with C_{TH} and L_G form a π section high-pass filter which isolates the low-frequency signal from the high-frequency port.

To examine ^1H efficiency, the double resonance circuit is reduced to the single resonant circuit, Fig. 3c, by shorting across C_{TX} and removing L_G, in which case the ^1H 90° pulse width is 2.3 μs (~50 W at 500 MHz). Removing the short across C_{TX} results in no increase, showing that, indeed, C_{TX} provides a good ground at the ^1H frequency. With 4-turn and 2.2-turn coils inserted for L_G, the ^1H 90° pulse width increases to 3 and 4 μs, respectively.

Summarizing the double resonance performance, with 4-

TABLE 1
Conditions for Matching and Tuning Three Channels

	Tuning	Matching
X1	$\omega_{X1} = \dfrac{1}{\sqrt{(C_{TX} + C_{MX})L}}$	$\dfrac{1}{Q\omega_{X1}^3 C_{MX}^2 L} = Z_0$
X2	$\omega_{X2} = \dfrac{1}{\sqrt{C_{TX} + C'_{TX} + C_{MX} + C'_{MX})L}}$	$\dfrac{1}{Q\omega_{X2}^3 (C_{MX} + C'_{MX})^2 L} = Z_0$
^1H	$\omega_{^1H} = \dfrac{1}{\sqrt{C_{TH}L'}}$	$\dfrac{Q'(\omega_{^1H} L_{MH})^2}{\omega_{^1H} L'} = Z_0$

Note. Q and Q' are the effective quality factors for the series (X1 and X2) or parallel (^1H) combination of L_S and L_G, respectively.

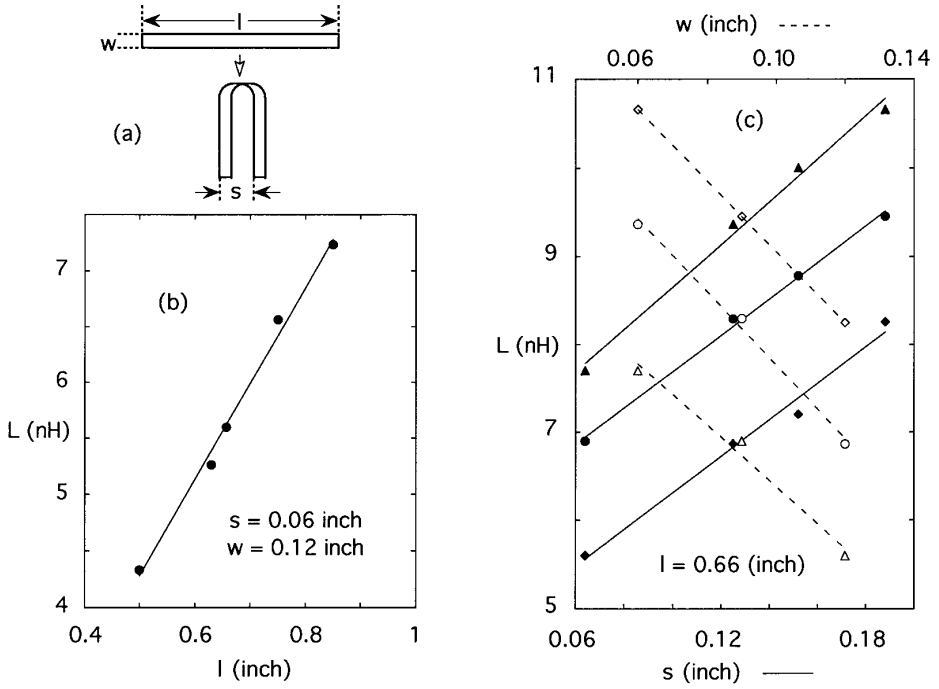

FIG. 4. Experimentally measured values of ''U''-shaped inductors. The dimensions l, w, and s are defined in (a). (b) L versus length, l. (c) L versus separation, s, for different widths; w = 0.12 inch (♦), 0.09 inch (●), and 0.06 inch (▲), and L versus w for different separations; s = 0.19 inch (◇), 0.12 inch (○), and 0.06 inch (△). Inductances were obtained by soldering the coil into the circuit of Fig. 3b with known capacitances and measuring the resonance frequency.

turn ($L_S \sim 80$ nH) and 2.2-turn ($L_G \sim 30$ nH) coils, the efficiencies of the X1 and ^{1}H channels are, respectively, essentially the same as and reduced by a factor of 2 compared to their corresponding single-frequency circuits. These values are in good agreement with those predicted from Eq. [3], and the actual component values are within ~20% of the calculated values, indicating that stray reactances are small. This circuit, with approximately the same inductances, has been used in a 5-mm MAS probe. The ^{13}C and ^{1}H 90° pulse widths are 4.0 μs (250 W at 125 MHz) and 4.5 μs (75 W at 500 MHz).

The circuit is tuned to a third frequency, $f_{X2} < f_{X1}$, by adding a capacitance, C'_{TX}, in parallel to the tuning capacitor with an intervening trap circuit tuned to f_{X1} (*4*), i.e., the circuit elements labeled A in Fig. 3a. Efficiency at f_{X1} is best when the resonant impedance of the trap ($Q\omega_{X1}L_P$) is large, while at f_{X2} the trap impedance ($\sim -i\omega_{X1}^2 L_P/\omega_{X2}$) should be small. To make the trap Q high, the inductor diameter is larger than the sample inductor (*10*). With L_P = 200 nH (5 turns, 0.28 inch × 0.38 inch), a short was placed across C'_{TX} and C_P is tuned so the resonance frequency f_{X1} is unchanged from the double-resonance circuit. The short across C'_{TX} is then removed and negligible change in f_{X1} is observed upon tuning f_{X2} by varying C'_{TX}.

The diplexer arrangement shown in Fig. 5 is added outside the magnet via a $\lambda/2$ line at f_{X1} to isolate the low-frequency channels and to impedance match the channel at f_{X1}. Impedance matching outside the magnet has been shown to result in a negligible decrease in probe efficiency (*9*). The bandpass filters are low-insertion-loss (0.4 dB), high-power commercial units (Trilithics, H5BE series, Indianapolis, IN). With proper choice of the inductors in the two trap circuits, the insertion loss at either frequency was less than 0.6 dB and the isolation between any two inputs was in excess of 90 dB. As a double resonance probe without the diplexer, ^{15}N and ^{13}C 90° pulse widths are increased by 15% and 25%, respectively, compared to their values in the double resonance circuit with no increase in the ^{1}H pulse width. As a triple resonance probe, the 90° pulse widths of ^{13}C, ^{15}N, and ^{1}H are 5.5 μs (125 W at 125 MHz), 5.5 μs (200 W at 50 MHz), and 3.4 μs (110 W at 500 MHz),

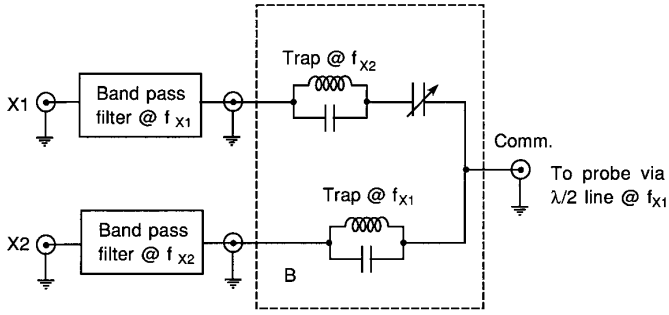

FIG. 5. The diplexer circuit placed outside of the magnet at an electrical distance of $\lambda/2$ at f_{X1} from the circuit shown in Fig. 3.

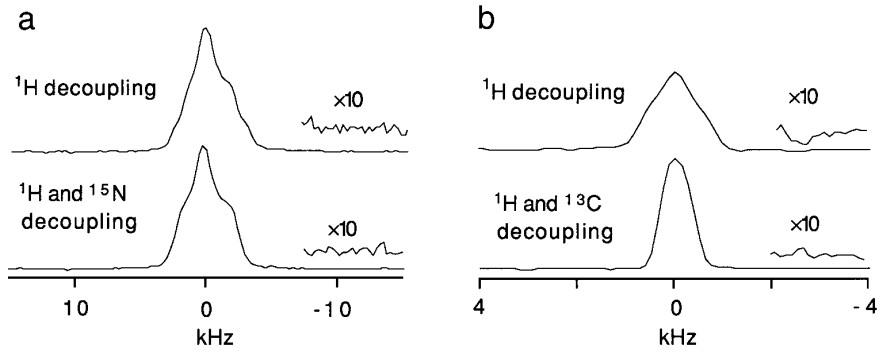

FIG. 6. Powder spectra of glycine-2–^{13}C–^{15}N. Insets show the noise levels expanded vertically 10×. See text for additional details.

respectively. No electrical breakdown is observed during a 4-ms proton decoupling period when the power is 110 W. ^{1}H decoupled ^{13}C (Fig. 6a) or ^{15}N (Fig. 6b) cross-polarization spectra of ~10 mg of glycine-2–^{13}C–^{15}N powder were obtained with and without ^{15}N or ^{13}C decoupling. Irradiation at the ^{15}N or ^{13}C frequency results in the expected narrowing due to decoupling of the ^{15}N–^{13}C interaction. Compared to the spectrum with only ^{1}H decoupling, signal intensities and noise levels are unchanged with 50-kHz ^{15}N or ^{13}C decoupling fields.

ACKNOWLEDGMENT

The authors express their appreciation to Dr. Carroll J. Hill for help in calculating the impedance of transmission lines.

REFERENCES

1. V. R. Cross, R. K. Hester, and J. S. Waugh, *Rev. Sci. Instrum.* **47,** 1486 (1976).
2. Y. J. Jiang, R. J. Pugmire, and D. M. Grant, *J. Magn. Reson.* **71,** 485 (1987).
3. F. D. Doty, R. R. Inners and P. D. Ellis, *J. Magn. Reson.* **43,** 399 (1981).
4. S. Kan, M. Fan, and J. Courtieu *Rev. Sci. Instrum.* **51,** 887 (1980).
5. H. Skilling, ''Electric Transmission Lines,'' p. 90, McGraw–Hill, New York (1951).
6. E. O. Stejskal and J. D. Memory, ''High Resolution NMR in the Solid State,'' Oxford Univ. Press, New York (1994).
7. E. Najim and J.-P. Grivet, *J. Magn. Reson.* **93,** 27 (1991).
8. P. Chien and G. S. Harbison, *Sol. State. Magn. Reson.* **7,** 343 (1993).
9. J. H. Walton and M. S. Conradi, *J. Magn. Reson.* **81,** 623 (1989).
10. ''Reference Data for Radio Engineers,'' 5th ed., Howard W. Sams & Co., ITT (1973).